Global available solar energy under physical and energy return on investment constraints

Elise Dupont[a,*], Rembrandt Koppelaar[b], Hervé Jeanmart[a]

[a] iMMC - Institute of Mechanics, Materials and Civil Engineering, Université catholique de Louvain, 1348 Louvain-la-Neuve, Belgium
[b] Ekodenge Sustainability Engineering, London SE1 8ND, England, UK

HIGHLIGHTS

- A novel grid-cell approach to estimate global solar energy potential.
- Solar potentials constrained by land-use, technology conversion and net energy.
- A new solar-to-electric efficiency parametrization for CSP power plants.
- Power plants design optimised by maximising the Energy Return on Investment.
- Solar potential is established between 1089 and 165 EJ/year at EROImin from 5 to 9.

ARTICLE INFO

ABSTRACT

The amount of energy striking the earth's surface in one hour is higher than global annual societies energy use, yet the fraction of incoming solar radiation that can be harvested is significantly constrained. A global grid-cell methodology was adopted to assess the available global solar energy potential taking into account four constraints: land-use, solar irradiation, solar-to-electric technology, and net energy. Net energy is the amount of energy that is delivered to end-users, after subtraction of the energy inputs needed for capital infrastructure and operation. Both photovoltaic and concentrated solar power technologies are considered. The resulting constrained solar potential worldwide was estimated at 1098 exajoules per year, of which 98%, 75%, and only 15% can be extracted if the system needs to deliver an energy return on energy invested set at 5, 7.5, and 9, respectively. The resulting global solar potential is substantially lower than most previous estimates. Depending on how high the energy return needs to be relative to the energy investment needed to maintain a sustainable society, the achievable potential will be significantly constrained. The effect is especially significant in lower solar radiation regions. The European Union holds only 2% of the global solar net energy potential.

1. Introduction

Despite negative impacts of fossil fuels on air pollution and climate change, and limitations to their low-cost resource base [1], the consumption of fossil fuels still continues to increase. In contrast, a sustainable future requires large scale expansion of renewable energies, mainly wind and solar, to supply the majority of current and growing energy demand [2]. Large disruptive change is needed to achieve such a transition [3]. At present under business-as-usual energy use scenarios, world primary energy demand is still expected to grow by 30% between today and 2040, whilst the share of renewable energies in the energy mix does not exceed 40% by 2040 [4].

A growing number of modelling scenarios have now been developed

that encapsulate the disruptive changes required to achieve a 100% renewable energy system by 2050 for 139 countries [5] and 145 regions with hourly simulated intervals [6]. In terms of solar power these require a scale-up to generate 380 EJ/year of solar electricity [6]. The technical feasibility of this scale-up under a 100% renewable energy system scenario has been put in doubt by other academics citing oversimplified assumptions [7]. A key claim is that 100% renewable energy scenarios assume too rapid technological progress and scaling up of renewable energy infrastructure, without a thorough assessment of underlying engineering and physical constraints [8], as well as energy systems aspects such as grid operation security parameters [9]. In global and regional energy scenarios a critical underlying parameter is the available renewable energy potential that can be harvested on a

---

* Corresponding author.
 E-mail address: elise.dupont@uclouvain.be (E. Dupont).

Table 1
Previous studies in the literature and the constraints included to assess the harvestable solar energy potential.

Study	Technical Potential [EJ/year]		
	Centralised PV	Rooftop PV	CSP
Hoogwijk M., 2004 [15]	1300	22	–
Trieb F., Schillings C. O'sullivan M., Pregger, T. Hoeyr-Klick C., 2009 [16]	–	–	10,605
Global Energy Assessment, 2012 [17]	6000–280,000	–	–
Castro C. de, Mediavilla M., Miguel, L.J., Frechoso F., 2013 [18]	60–120		
Deng Y. Y., Haigh M., Pouwels W., Ramaekers L., Brandsma R., Schimschar S., Grozinger J., Jager D. de., 2015 [19]	316–2815	210	131–1078
Jacobson M.Z., Delucchi M.A., Bauer Z.A.F., …, Wang J., Weiner, E., Yachanin A.S., 2017 [5]	41,461	47	31,104

sustainable basis [10]. It is critical to accurately estimate this potential of renewable energies by taking into account constraints to energy extraction, including land use constraints [11], physical availability constraints [12], socio-economic scaling constraints [13], and limitations of the energy efficacy of generating systems to deliver energy to society [14].

This study contributes to the literature by providing a novel comprehensive multi-constraint methodology to assess the potentially available renewable solar energy that can be sustainable harvested, and by exploring the global and regional results of this novel methodology. Similar previous studies as summarised in Table 1 provided wide ranging results. Substantial variations exist in methodology and crucial differences in assumptions. Studies hitherto primarily assessed land cover constraints and solar irradiance estimations. This study is the first to carry out a multi-constraint analysis for the net solar energy potential that takes into account land use constraints, physical available energy constraints, and constraints by requiring the delivery of a minimum amount of net energy to society, calculated using the Energy Return on Energy Invested (EROI) indicator. It also is the first study that incorporates the trade-offs between solar photovoltaic and concentrated solar power technologies, instead of analysing technologies in isolation, resulting in a much improved estimation then previously available. The results are usable for creating more realistic scenarios for the deployment of solar technologies for individual geographies and countries by taking into account a more realistic estimate of the solar resource available.

The adopted dimensionless indicator for the applied net energy constraint, the Energy Return On Investment (EROI), was originally developed in the 1980s [20]. It is defined as the ratio between the energy output of the facility in the nominator, and the energy inputs required to establish, operate, and decommission energy generating infrastructure over its lifetime in the denominator [21]. The ratio can be expressed in descriptive form as:

$$EROI = \frac{Gross\ Energy\ Produced}{Local\ Energy\ Inputs + Upstream\ Energy\ Inputs} \quad (1)$$

The rationale for net energy analysis and its use of EROI was established to evaluate how much energy is used by the energy sector itself, and how much energy is available to produce non-energy economic outputs. It is pertinent to calculate constraints of renewable energy like solar facilities, as the EROI of these facilities decrease with their spatial expansion, since the sites with the best available resource are exploited first [22]. A society that can only access energy resources with a low EROI is an energy harvesting society, as it requires an energy sector that is a significant proportion of the entire economy, leaving a much smaller energy surplus for other sectors to deliver basic human needs and luxuries [23]. The consequence of shrinking EROI during an energy transition, is that more and more resources in terms of physical capital and associated labour will be required for every marginal energy supply addition. With a decreasing EROI, more and more energy will need to be diverted from other sectors of the economy to feed the energy sector [24]. Based on this logic another deduction can be made that there is a minimum average EROI level across energy generation

infrastructure that is needed to maintain industrial societies at current consumption levels [25]. If not attainable, it can be deduced that a decrease in the EROI harvested by a society will lead to a decrease in living standards, as less energy will be available on a net basis to support the production of non-energy sector goods and services [26]

Recent proposed refinements of the EROI calculation methodology include the incorporation of self-consumption of power plants also referred to as parasitic load [27], time value discounted EROI [28], and the distinction between energy inputs that are obtained externally to or internally as a consequence of an energy generating process [21]. The distinction is relevant to adequately evaluate the net energy potential of fossil fuel sources in cases where such sources utilise their own resource to generate energy for society, such as the tar sand resources in Canada [29].

2. Methodology

To derive a more precise estimate of the global solar energy potential, a grid cell model was developed to divide the globe into cells with a resolution of $0.1° \times 0.1°$ (cells of $100\ km^2$ on average), resulting in a model with over 5 million grid cells. The multi-criteria constraints model selects which cell area is available for solar energy generation (geographic constraints), how much solar radiation is incoming in each cell (solar resource constraints), what share of solar energy photons are captured and converted into heat and electrical energy (solar technology constraints), and what share falls under or above a set EROI threshold (Net Energy constraint). The five technologies that were evaluated include polysilicon solar-PV (poly-Si-PV), monosilicon solar-PV (mono-Si-PV), parabolic-through CSP technology with a heat transfer fluid (PT-oil), parabolic-through CSP technology using molten salt thermal energy storage (PT-salt-TES), and solar power towers with salt thermal energy storage (ST-salt-TES). For an overview of solar technologies and their physical system descriptions the review paper of Kumar and Kumar [30] can be consulted.

The model uses an optimization algorithm so as to find the upper limit of energy that can be generated within these sets of constraints for each technology, reflecting the theoretical maximum within a series of realistic constraints. The grid size of the model was selected to establish a parsimonious model that delivers a sufficiently accurate spatial granularity at a reasonable computational time. The readers can find details on the grid cell multi-constrains model setup in the author's previous work on the global net wind energy potential [31]. Specific aspects and parameters for establishing solar-PV and solar-CSP technology theoretical potentials are elaborated upon in Sections 2.1 to 2.6 based on seven modelling steps (Fig. 1) as outlined:

1. A **suitability factor** for solar energy is associated to each cell, discussed in Section 2.1, in order to take into account geographical constraints.
2. The availability of **solar energy** in each cell are assessed, as described in Section 2.2, to establish solar resource constraints.
3. The **conversion efficiency** of available solar energy flux into electricity is assessed, as well as the ground cover area of the complete
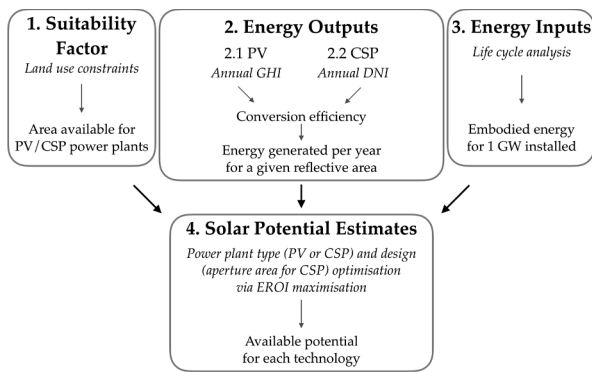
Fig. 1. Simplified overview of the methodology used to evaluate the global available solar potential.

systems, as described in Section 2.3, to take into account solar technology constraints.

4. The **energy inputs** for each type of solar plants are evaluated as described in Section 2.4.

5. The **scaling of CSP plants** collectors to fit with maximum power production was established relative to the power block rating and storage capacity, as described in Section 2.5.

6. Based on the findings from Sections 2.2 and 2.4 **the net energy and EROI** values of each solar technology and grid cell was subsequently calculated, as described in Section 2.6

7. A EROI threshold limit was then applied to derive**EROI dependent estimates of the net energy potential**at a global scale, as per Section 2.7, resulting in an integration of geographical, solar resource, solar technology, and net energy constraints.

In general the selection of parameter values has been carried out based on criteria for consistency by using where available global standards, studies that have a consistent coverage of a majority of countries and geographies, and review studies that use a meta-analytical method. Each section outlines specific parameter values and how they were estimated or obtained from previous studies. Whilst as much as possible country or geography specific values were evaluated or calculated, in certain cases averages were still utilised that were deemed representative enough to cover different geographies based on the literature.

2.1. Geographic constraints

Since a majority of land mass is not suitable for solar power deployment, realistic assumptions should be taken regarding the available area to account for geographical constraints. To incorporate this for various technology types, solar technologies are divided in the multi-constraint model in large-scale applications, i.e. power plants of several megawatts; and smaller kilowatt size rooftop solar PV panel systems. Geographic criteria for both differ since these two kinds of applications do not compete for the same land area. For large scale megawatt plants, a suitability factor is associated to each grid cell, defined as the cell's fraction suitable for a CSP and a PV solar power plant installation.

The suitability factor was determined usng a three step process. First, the types of land use suitable for large scale megawatt plant deployment are selected, using similar assumptions as previously made by the authors [31] adapted to solar power constraints. Land cover of each grid cell was retrieved from the GlobCover 2009 dataset, created by the European Space Agency (ESA) and the University catholique de Louvain (UCL) which classifies global land cover in 22 classes, at a 10 arc-second resolution [32]. Bioreserves from the world database on protected areas [33] are excluded, as well as urban areas and relatively remote and unpopulated areas (Antarctica, Greenland and small remote islands). To assing countries to each grid cell the dataset from [34] was utilised.

The second step was to take an approximation of the share of available land for those land use types where large solar power plants could be deployed. The share was set at between 5% to 10% of global area depending on the land use type for land with suitable land use and slopes (see Table 2) [15]. Large scale solar power plants are difficult to combine with other land uses, beyond a few exceptions such as sheep grazing, therefore the suitability factor should be significantly lower [35]. Note that these parameter values are rough approximations and are unlikely to be representative across geographies for different land uses. More precise GIS based estimations have been developed, but have not yet deployed to create country by country assessments.

The final step was to apply exclusion criteria based on terrain slope [36]. CSP plants are not suitable for areas with an average slope greater than 2% [16], while PV plants may be placed in areas with slopes up to 30% (~16.7°) [19]. The global terrain slope and aspect database from IIASA was used, which provide 8 classes of terrain slope gradients [37]. A total of 38% of land area (47 millions km^2) has an average slope below or equal to 2%, and 87.5% of the total land area (107 millions km^2) has an average slope above or equal to 30%.

For kilowatt scale rooftop applications a separate methodology was used based on estimates of available rooftop area in m^2 for each country in the world. The only available globally applicable dataset to the knowledge of the author's of rooftop area for residential and commercial buildings covering 139 countries has been developed by [5] which is adopted for this study. Their estimates are calculate rooftop area based on floor area per capita adjusted for the number of building stories, the population, a rooftop slope adjustment, and a building overhang adjustment. Calculated floor area per capita was estimated by [5] using a regression equation validated with EIA data for the US and the Entranze floor area database for EU countries [38]. After rooftop area is calculated the proportion suitable for solar-PV can then be defined based on a usability factor, so as to take into account orientation and shading restrictions. Three methods with varying complexity have been created to present to estimate the suitability factor which were reviewed by NREL [39] covering 35 studies, that cover estimates for a subset of geographies such as individual cities or countries. The resulting average usability factors used here based on NREL's meta-review is 65% for commercial rooftops and 25% for residential rooftops for solar-PV [39]. The values are not extensively analysed and further research would be needed to assess the suitability of these factors, and ideally to generate a country by country specific listing of roftop usability factors.

The total geographic constraints that result in area per land use type suitable for solar-PV and CSP deployment is outlined in Table 2 (Fig. 2).

Table 2
Repartition of the available areas into land use categories with a land use factor and slope evaluation.

| Land Cover	Land use factor [%]	Area [10^6 km^2]
Sparse vegetation, grassland, barren areas	10	37
Forests	0	32.4
Croplands	10	7.6
Shrubland	10	8.5
Mosaic vegetation - croplands	5	17.9
Mosaic grassland - forest or shrubland	5	6.9
Urban Areas	0	0.32
Water bodies	0	11.9
Total		**122.5**
Protected Areas	0	17.8
Slope > 2%	0 (CSP)	69.6
Slope > 30%	0 (PV & CSP)	9.4
Suitable for solar-PV plants		**5.4**
Suitable for CSP plants		**2.7**
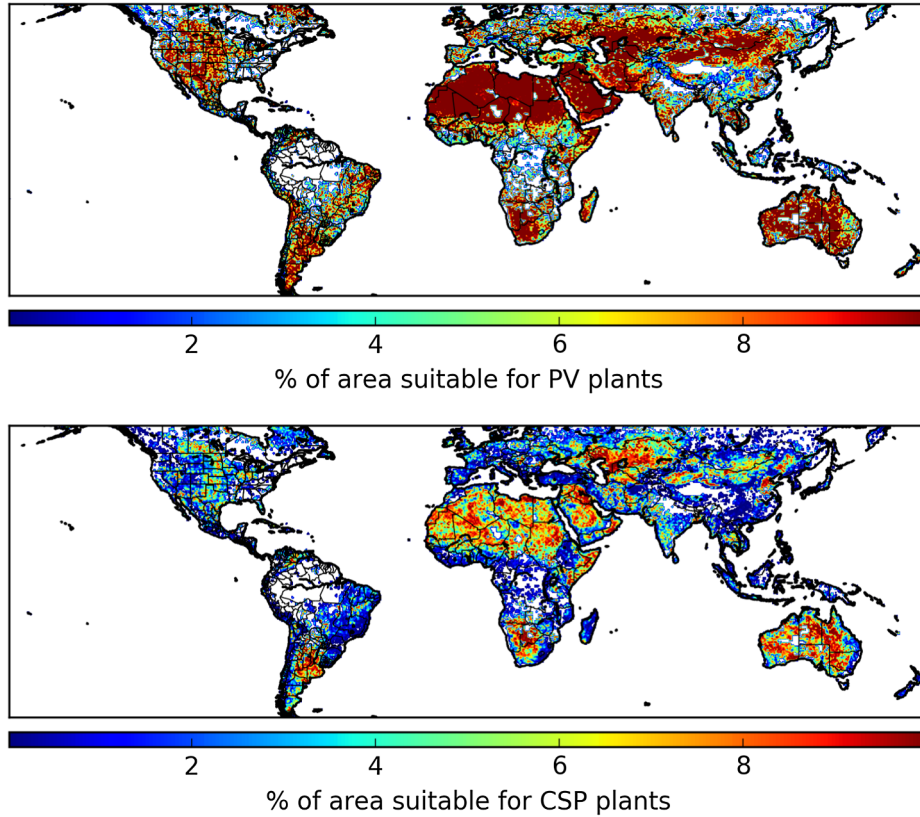
Fig. 2. Proportion of the area suitable for centralised solar power plants (from 0 to 10% of a cell's area).

2.2. Solar resource constraints

To calculate solar power output, a general formula was employed to establish physical constraints and solar technology constraints, so as to establish average power output per unit of area:

$$P_c = A_c \cdot I_c \cdot \eta \cdot \text{GCR} \quad [\text{W/m}^2] \tag{2}$$

With:

- P: power output of the solar technology system for a grid cell c in watts.
- A: applicable ground area for a cell in the grid model derived from Section 2.1.
- I: the yearly averaged irradiation [W/m^2] in GHI for PV and DNI for CSP for a cell in the grid model.
- η: the conversion efficiency as the ratio of the electricity output to the solar irradiance of the CSP and PV technology systems.
- GCR (Ground Cover Ratio), the ratio of the surface occupied by the PV cells or solar collectors to the total ground area occupied by the solar power plant.

To obtain data for parameter I, data for global horizontal irradiation (GHI) and direct normal irradiation (DNI) was used as input in the multi-constraints model. Global Solar Atlas data was used, which contains values with a resolution of 30 arcsec (approximately 1 km) [40]. To estimate yearly averages up to 20 years of data were captured with daily GHI and DNI totals (Fig. 3). Global Solar Atlas is a global standard funded by the World Bank developed under the ESMAP initiative on renewable energy resource mapping [41]. Outputs of the Global Solar Atlas have been validated using measurement data with over 200 high quality ground measurements in all continents.

2.3. Solar technology constraints

2.3.1. Solar photovoltaic conversion

The full cycle conversion efficiency η for solar-PV in equation X is calculated for each grid cell using the estimated electricity produced by a solar system, relative to the incoming solar radiation per grid cell. The electricity produced after n years of operation for a solar-PV system is calculated as:

$$E_n = \sum_{i=0}^{n-1} \eta_{STC} \cdot p_r \cdot H_{\text{yearly}} \cdot (1-\alpha)^i$$
$$= \eta_{STC} \cdot p_r \cdot H_{\text{yearly}} \frac{1-(1-\alpha)^n}{\alpha} \tag{3}$$

With H_{yearly} the average annual global irradiation (kWh/m^2/year), α the degradation rate, η_{STC} the efficiency of solar modules measured under Standard Test Conditions (STC), and P_r the ratio of the actual performance of the system to its performance under STC. The duration of operation was taken at 25 years based on solar-PV module warranties or performance guarantees. The efficiency of solar modules is measured by manufacturers under Standard Test Conditions (STC) and defined as the nominal power of a photovoltaic panel expressed in watt-peak, W$_p$. STC are an irradiance of 1 kW/m^2 with a cell temperature of 25° and a solar irradiation angle of 45 degrees. The conditions correspond to a spectrum similar to sunlight hitting the earth's surface at latitude 35°N during the summer period [42].

The estimated efficiency of solar modules deployed in 2018 has been estimated at 17.7% based on a global PV project database taking into account the impacts of fixed tilt and tracking on efficiency [43]. The value is aligned with an estimated average efficiency of 19% for polysilicon cells sold by producers found in the International Technology Roadmap for Photovoltaic (ITRPV) for 2018, taking into account lower efficiencies for modules versus individual cells [44]. ITRPV estimates are based on survey data from 55 solar supply chain companies from China, Germany, Spain and the United States [44]. Based on these
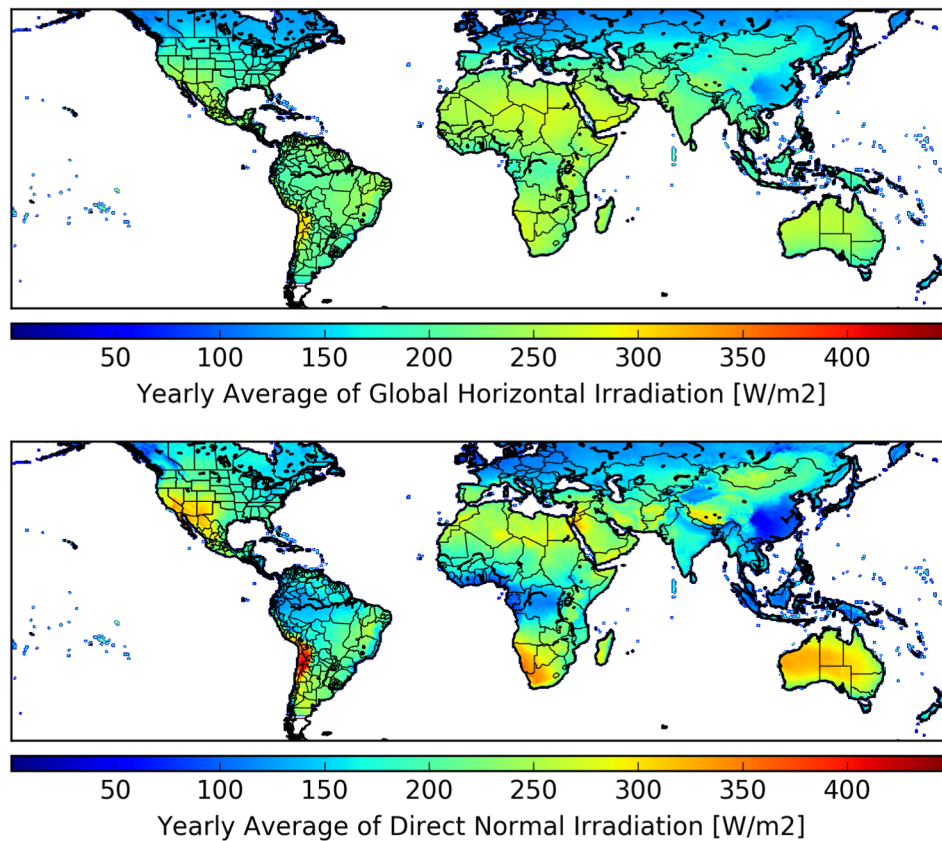
Fig. 3. Longterm yearly average of global horizontal irradiation (GHI) and of direct normal irradiation (DNI), data obtained from the Global Solar Atlas.

values for this study a 17% efficient solar value was taken for the poly-Si-PV technology to reflect current technologies. An efficiency of 17% corresponds to 170 W_p/m^2, whereby 1 kW_p would occupy 5.9 m^2.

In case of mono-Si-PV technology a higher cell efficiency was taken to reflect upcoming cell technology with significantly improved efficiency, including passivated emitter and rear cell (PERC) designs and heterojunction cells [45]. The reason for incorporating such values is to adequately take into account likely improvements to have a better estimate for the conversion constraint for solar-PV technologies The average efficiency of mono-silicon cells sold in 2018 was estimated at 21.5% based on industry surveys carried out by industry body ITRPV, with PERC designs incorporated in 35% of mono-silicon cells, and heterojunction designs in < 1% of sold cells [44]. Industry expectations include heterojunction solar cells of n-type to gain a market share of 15% by 2029 with an average cell efficiency of 25%, and PERC cells to gain a market share of 70% with average cell efficiency on the market of 23.5% and 24% for p-type and n-type mono-Si [44]. The industry expectations are aligned with 24.7% and 25.1% efficient HJS mono-silicon cells that have been developed by Panasonic and Kaneka respectively, at pilot scale [45]. Based on these evaluations a module efficiency of 24% was utilised for mono-Si-PV technologies as a reasonable estimate for conversion efficiencies that will be reached around 2030.

The real-life output of a solar-PV plant is further influenced by optical, array and system losses, independent from the location and the panel orientation. Recommendations for the Performance Ratio (PR) has been established in the global methodology guidelines on life cycle assessment of photovoltaic electricity developed by the International Energy Agency. Based on a literature review a default PR value of 75% was recommended for roof-top and 80% for ground-mounted utility installations [46]. The recommendations are corroborated based on an evaluation of 30,000 solar-PV systems with data from 2006 and 2014 located in France, UK, Belgium and Spain [47]. The analysis applied a

Weibull distribution with individual systems ranging from 60% to 90% at extremes when looking at data from a large sample of solar-PV plants, with a mean and median around 80%. Typical performance ratios were established as the mode of the distribution at 81% for the UK, 80% for Belgium, 78% for France, and 81% for Spain. The data for Spain covered mostly large-scale PV plants versus rooftop systems for the other countries. An analysis of the performance ratio of 7000 solar-PV systems in the UK using data from 2002 and 2013 established a typical performance ratio of 83% as the mode of the data distribution across all systems [48]. An analysis for Germany evaluated the PR for 100 rooftop solar-PV systems and found a median PR of 84% [49].

Meta-reviews of many systems in other climate geographies were not found in the literature, yet individual system analyses are available. The PR of four large megawatt scale solar power plants in Thailand were evaluated obtaining PR's between 75% and 80% when regularly cleaned, dropping by up to 5% if dust is not cleared on a timely basis [50]. The performance of three kilowatt scale solar-PV systems in Peru was evaluated finding PR ratio's at 84%, 82% and 74.5% respectively [51]. An 11 kilowatt-peak scale solar-PV plant in Iran was evaluated finding a PR of 80.8% for mono-Si PV and 83% for poly-Si PV [52]. The PR for a solar-PV system of 8 kiloWattpeak in Nanjing, China was evaluated at 75% to 85% for mono-Si pV and poly-Si PV varying per month of the year [53]. PR analyses for India established values of 72% for a 20 MW solar-PV plant [54], 74% for a 190 kiloWatt peak plant [55], 82.7% for a 186 kiloWatt peak plant [56], 77% for a 5 kiloWatt peak rooftop system [57], and a 77% PR rating for a 25 MW plant [58]. A PR for a 3.2 kW solar-PV system in South Africa was established at 84% [59]. The performance of a mall kilowatt scale rooftop system in Ghana was studied finding a PR of 68% for mono-Silicon and 76% for poly-Silicon technologies [60]. Based on the evaluation of the studies above the PR recommended by the IEA was found to be similar to those established from more recent meta-studies and individual systems in various geographies and climate zones. The use of average PR ratio for

different geographies is thereby a reasonable assumption, and the recommended performance ratio by the IEA of 80% was applied in this study.

The degradation rate is included to take into account performance decline over time caused by smaller or larger failures of technology components [61]. An extensive literature review of 2000 studies with published degradation rates since the 1960s covered values from all continents, with most data points from the US, Europe, Japan and Australia [62]. Their median degradation rate for mono-Si modules was established at 0.47% for installations before 2000 and 0.36% for installations after 2000, and for poly-Si modules at 0.61% for installations before 2000 and 0.64% for installations after 2000. Based on this evaluation a value of 0.5% per year was utilised in this study for the solar PV conversion calculation.

The full cycle conversion efficiency η was based on these parameters established at 13% over 25 years for a cell efficiency of 17%, a performance ratio of 80%, and a degradation rate of 0.5%, the average efficiency of the system over 25 years would be 13% (18.6 for a 24% efficiency panel).

2.3.2. Concentrated solar power conversion

The conversion efficiency η for CSP plant was established as the product of the efficiencies of the solar field, of the receiver technology, and of the power block:

$$\eta_s = \eta_{\text{field}} \cdot \eta_{\text{receiver}} \cdot \eta_{\text{power block}} \tag{4}$$

The efficiency of the solar field is defined as the ratio of the incoming solar radiation that is transferred as heat to the heat transfer fluid. It includes optical and geometrical losses including cosine effect, row-to-row shading, and soiling. The receiver efficiency mainly includes thermal losses, for example due to loop piping for parabolic through CSP. In total the thermal efficiency of the solar field has been evaluated around 35–40% [63]. The power block efficiency depends on the temperatures of the steam cycle and is established at ~40%, depending on the temperatures reached.

The full cycle solar-to-electric efficiency is currently 15% for parabolic through technologies, and 20% for power tower technology [64]. Efficiency increases with the level of irradiance with measurements of 12% at $1800\,\text{kWh/m}^2\text{/year}$ and up to 16% at $4000\,\text{kWh/m}^2\text{/year}$ in [65].

Unlike PV plants, where the efficiency does not vary with the size of the installation, the design of CSP plants must be optimised due to the fixed size of the power block. The main parameter to optimise is the total aperture area (total reflective surface), i.e. the optimal number of concentrators (mirros/heliostats) for a given rated power and storage capacity. First, the area needed to produce the power block rated power at a design point (in general $950\,\text{W/m}^2$ of direct solar irradiance at solar noon on the summer solstice) is estimated, and then a multiplication factor, the solar multiple, is applied to the calculated area in order to take into account lower irradiation levels and storage needs. Typical values for the SM range from 1.3–1.4 (plants without storage) to 2.7 for 12 h of storage [66].

$$\text{Aperture Area [m}^2\text{]} = \text{SM} \frac{\text{Rated Power [W]}}{\eta_{\text{design}} \cdot \text{DNI}_{\text{design}} \ [\text{W/m}^2]} \tag{5}$$

Therefore, for a given rated power of the power block, the solar multiple is the parameter that must be adapted to the annual average DNI and latitude of a location. According to Eq. (5), the reference area (corresponding to a SM of 1) for a power block of 1 MW and an design efficiency of 22% would be 4785 m^2.

Increasing the aperture area above the reference area allows to increase annual production (hence changing the capacity factor), but it also decreases the solar-to-electric conversion efficiency of the plant. Given the fixed power block rating power, oversizing the aperture area increases the risk of curtailment during hours with high direct solar

radiation. In addition, increasing the aperture area also increases energy dissipation (thermal losses due to longer pipes for parabolic trough, and optical losses with increasing distance to the receiver for power tower).

In order to model the evolution of the efficiency with the aperture area and location, simulations were run with the NREL System Advisor Model [67]. For a representative number of locations and solar multiples, the annual energy production of CSP plants was estimated and the annual solar-to-electric efficiency was calculated. The simulation results are presented in Section 2.5.

2.3.3. Solar technology ground cover ratio

The ground cover ratio parameter in Eq. (2) covers the total spatial requirement of large scale solar-PV and concentrated solar power plants relative to the area of the solar panels and concentrating mirrors. According to [65] the ground cover ratio is 20% for PV plants and 13.5% for CSP plants. As a result solar PV power plant including all infrastructure covering access roads and space for logistics occupies 5 times the area of the PV panel alones. And 7.5 times the area of the concentrating mirrors is used for a CSP plant. The values are similar to the results of an analysis of existing, under construction and proposed utility-scale facilities in the United States conducted by NREL [68]. The evaluation of land-use requirements of 32 utility-scale PV plants and 22 CSP plants yielded an average ground cover ratio of 19.5% for solar PV and 15.5% for CSP. In the multi-constraints model the values established by [65] are utilised. Finally, for rooftop applications, a spacing factor is already included in the usability factor described in Section 2.1.

2.4. Solar energy inputs

Many existing studies calculate the EROI using life-cycle approaches for solar-PV modules, and only a few have studied the EROI of CSP. A meta-analysis for solar-PV was published by [69] and for CSP by [70]. Study results vary due to different boundary and technology assumptions and age of manufacturing input data. Existing results are advanced by taking a complete cradle-to-grave boundary approach, encompassing nine stages from raw materials to final decommissioning, similar to [27], including (i) raw materials extraction and conversion to an intermediary material (such as aluminium rolls), (ii) transport to the factory, (iii) manufacturing of the energy technology and other components, (iv) transport to the installation site, (v) installation, (vi) operation, (vii) maintenance, (viii) decommissioning, and (ix) decommissioning transport. Values include both operational and embodied energy from raw materials extraction and processing.

Data values are presented for 1 GW of 17% efficient poly-Si-PV, 24% efficient mono-Si-PV, PT-oil, POT-salt-TES, and ST-salt-TES. The reference of 1 GW was arbitrarily chosen, and does not reflect the current or expected size of the facilities. All electricity values, except for operational parasitic load, were converted into primary grid inputs, to obtain a fuel energy equivalent EROI value, also referred to as primary energy equivalent [71]. The electricity to fuel conversion was carried out by multiplication with a factor of 2.42, indicating that, globally, 2.42 GJ of fuel is required at present to produce 1 GJ of electricity. The value was obtained by weighting the electrical to primary efficiency of each power source based on their share of produced power in 2018 from global electricity mix data derived from [72] and primary to electrical efficiencies for each power source data per source derived from [4], as described in Table 3. The used values are representative for solar systems integrated in a fuel based energy system. In contrast a fully 100% future renewable scenario study would assume a 1.0 multiplication factor.

2.4.1. Solar-PV life cycle data

The main components of a solar-PV plant are solar modules, inverters, internal cables and a transformer station. A solar module is

Table 3
Estimation of global primary to final conversion factor. Source of data: [72,4], this study.

Power source	Share of produced power (2018)	Electrical efficiency to primary (fuel) efficiency
Coal	37.95%	2.94 GJ/GJ
Oil	3.02%	3.13 GJ/GJ
Natural Gas	23.23%	2.70 GJ/GJ
Nuclear	10.15%	3.03 GJ/GJ
Hydro-power	15.75%	1.00 GJ/GJ
Bio-energy	2.35%	3.85 GJ/GJ
Wind Power	4.77%	1.00 GJ/GJ
Solar Power	2.20%	1.00 GJ/GJ
Other Renewables	0.58%	1.00 GJ/GJ
Total	**100%**	**2.42 GJ/GJ**

composed of solar cells, a film for protection typically made of EVA or Tedlar, glass, an aluminium frame and electronics. Six stages can be distinguished in the production of solar modules, (i) extraction of quartz, (ii) processing into metallurgical silicon, (iii) upgrading to solar grade silicon, (iv) manufacturing of wafers from silicon ingots, (v) transformation of wafers into solar cells, (vi) assembly of solar modules from all components. In addition to these manufacturing stages other phases in the life cycle are included. Table 4 summarizes the energy inputs associated with each stage in the life cycle. The calculation are based on the material needed, the estimated transport distances for each stage, and the energy intensities for materials extraction and transport calculations.

Data is presented firstly for poly-Si-PV based on a 17% efficient solar module as a lower limit solar-PV efficiency technology, and secondly presented for mono-Si-PV based on 24% efficient modules as a reasonable upper limit solar-PV scenario at efficiencies expected by the industry in 2030s, as discussed in detail in Section 2.3. The 24% efficient technologies include input data for hetero-junction mono-silicon manufacturing with ultra-thin amorphous layers (HJS) [73]. Materials data and manufacturing energy inputs data for metallurgical silicon to silicon modules manufacturing was obtained from recent studies covering Chinese factories for state-of-the-art mono-Si technology [74] and poly-Si technology [75]. Materials and manufacturing data for the additional HJS cell processes, namely amorphous layer deposition PEVCD (plasma enhanced chemical vapor deposition) process and transparent conductive oxide (TCO) sputtering, was taken from [76]. For a detailed methodological description the reader is referred to [77]. To cover installation materials for ground-mounted solar, the most common mounting infrastructure for solar-PV panels was taken, using galvanized steel based on pile driving, as opposed to concrete ballast systems. All other life cycle energy values were calculated using the parameters in a recent comprehensive study by one of the authors where further details can be found [27].

Energy inputs for solar-PV systems are dominated by extraction and

processing of minerals (about 60% of inputs), the manufacturing of the solar modules (about 30% of inputs), maintenance (about 7% of inputs), and operational parasitic load (1% of outputs). About 35% of fixed energy input is electricity converted into primary energy based on the earlier 2.42 GJ:GJ factor. The implication is that if the supply chain were to be based on a fully renewable system where such conversions are not occuring, the fixed energy inputs would be reduced by 20%. Fixed inputs being defined as inputs from raw material to decommissioning that are capital related (e.g. as opposed to operational inputs).

2.4.2. CSP life cycle data

Parabolic trough systems are composed of curved solar mirrors usually made out of tempered glass, a HTF pipe system with receiver pipes, and a power plant system. Solar power tower systems are composed of a central tower with a receiver, a field of heliostat flat solar mirrors that focus on the receiver, and a power plant system. Data is presented for three systems, including PT-oil, PT-Salt-TES, and a ST-Salt-TES, as outlined in Table 5 for each stage of the life cycle.

The basic PT-oil without storage is based on an oil HTF system. It represents the until recently commonly installed technology and is based on NREL data for the System Advisor Model [78], adjusted to exclude thermal storage. Based on the work of [79] a solar multiple (SM) of 1.3 was taken for capacity of the parabolic throughs, indicating that the field is slightly oversized relative to the power block.

The ST-Salt-TES also utilises NREL SAM data, which is based on the Ivanpah 377 MW plant in California, USA. The heliostat data is derived from BrightSource Energy's LH-2.2 heliostat [78]. Storage is based on a tank system with a molten salt mixture including sodium nitrate and potassium nitrate. The system was scaled based on the work of [79] with a SM of 2.7 to account for 12 h of thermal energy storage, indicating that the field is substantially oversized relative to the power block. A 35% thermal to electric storage efficiency was assumed [80].

The PT-Salt-TES represents a next-generation technology. A state of the art trough design is taken based on thin 1 mm steel sheets coated with a reflecting polymer film [81]. The storage system is based on polymer encapsulated phase change salts, which increases thermal conductivity and thus increases energy density and reduces salt storage needs [82], with materials and embodied energy costs taken from [83]. Energy for the manufacturing of heat transfer fluids was obtained from [84]. All other components are assumed similar to that outlined in [78]. Similar to the ST-Salt-TES a SM of 2.7 and a 35% thermal storage to electricity efficiency is assumed [79].

Energy input data in Table 5 are presented for the materials needed for the default aperture area for an installation of 1 GW: 6,22 km² for PT-oil and 12,9 km² for PT-Salt-TES and ST-Salt-TES (corresponding to a solar multiple of 1.3 without storage and 2.7 for 12 h of thermal storage capacity). This distinction allows to easily scale up or down the energy inputs for the mirror field, given the optimal aperture area calculated for each location and technology.

Table 4
Summary of life cycle energy inputs for solar-PV technologies.

	poly-Si-PV			mono-Si-PV		
	[GJ/GW]	Share [%]	Source	[GJ/GW]	Share [%]	Source
Raw material extraction & processing	12,211,500	65	[27]	8,880,750	55	[27]
Raw & intermediary material transport	33,930	0.2	[27]	24,660	0.2	[27]
Power plant manufacturing	4,394,480	23	[75]	5,596,460	35	[74,75]
, Construction material transport	303,480	2	[27]	218,450	1	[27]
Facility construction	71,650	0.4	[27]	61,280	0.4	[27]
Facility maintenance	1,322,800	7	[27]	1,131,300	7	[27]
Facility decommissioning	71,650	0.4	[27]	61,280	0.4	[27]
Decommissioning material transport	315,520	2	[27]	226,150	1	[27]
Total Energy Inputs [GJ/GW]	18,725,010	100		16,200,320	100	
Facility operation [GJ/GJ]	0.0097			0.0097		

Table 5

Summary of life cycle energy inputs for CSP technologies. Sources of data iincluding [78] for PT oil, PT-Salt-TES, and [83,78] for ST-Salt-TES.

	PT-oil		PT-Salt-TES		ST-Salt-TES	
	[GJ/GW]	Share [%]	[GJ/GW]	Share [%]	[GJ/GW]	Share [%]
Raw material extraction & processing	10,775,620	50	30,350,790	70	24,891,800	67
Raw & intermediary material transport	63,650	0.3	116,630	0.3	108,510	0.3
Power plant manufacturing	6,735,420	31	4,412,440	10	3,642,820	10
Construction material transport	517,960	2	1,494,040	3	1,222,840	3
Facility construction	106,000	0.5	220,160	1	220,160	1
Facility maintenance	2,673,540	12	5,511,600	13	5,511,600	15
Facility decommissioning	114,400	1	237,600	1	237,600	1
Decommissioning material transport	630,320	3	1,156,100	3	1,049,220	3
Total Energy Inputs [GJ/GW]	21,616,910	100	43,499,360	100	36,884,540	100
Facility operation [GJ/GJ]	0.073		0.073		0.073	

The energy inputs for CSP are dominated by extraction and processing of minerals (50% of inputs for installations without storage, up to 70% with storage), power plant manufacturing (30% of inputs without storage (mainly due to the oil HTF), and 10% with storage), the maintenance (12–15% of inputs), and the operational parasitic load (7% of the outputs).

About 15% of fixed energy input is electricity that is converted into primary energy based on the earlier 2.42 GJ:1 GJ factor. It means that in a fully renewable scenario fixed energy inputs would be reduced by 10%.

2.5. Establishing efficiency and CSP collector aperture area relation per grid cell

To provide for an upper theoretical limit for CSP technologies within constraints, the optimal ratio between solar collector field size (aperture area) and the power block and storage system needed to be established. To this end a relationship was established for the evolution of the solar-to-electric conversion efficiency with the average DNI of the location and the solar multiple of the plant. The end result is an understanding of the solar multiple for each cell that results in the optimal conversion from solar energy to electricity.

In order to do so, first 400 representative locations over the world were selected in the System Advisor Model (SAM) [67], and, for each, the annual output of a power plant was simulated for a set of solar multiples, around the values usually applied in existing power plants, which are based on economic evaluations (1.3 without storage and 2.7 with 12 h of thermal energy storage). The dependence of latitude on CSP efficiency was neglected in our study, as in [16], as no empirical relationship for the evolution of efficiency with latitudes has been established to present.

For each simulation, SAM estimates the annual production of the plant based on hourly resolved irradiance data. The solar-to-electric efficiency is calculated afterwards, based on the average DNI of the location and the aperture area (size of the collector field):

$$\eta_{\text{solar}\rightarrow\text{elec}} = \frac{\text{Annual Production [kWh/year]}}{\text{Aperture Area [m}^2\text{]}\cdot\text{DNI[kWh/m}^2\text{/year]}} \tag{6}$$

To find a regression function for the dependence on DNI and the solar multiple, first the evolution of the efficiency with DNI was studied for a fixed value of the solar multiple. The simulation points exhibit a logarithmic dependence of type $\eta = a\ln\text{DNI} - b$, as one can observe in Fig. 4.

The parameters a and b were estimated with a least squares linear regression (R^2 between 0.5 and 0.75).

Second, the evolution of the parameters (a and b) with the solar multiple was then studied. The range of the solar multiple was simulated from 0.9 to 2 without storage, and from 2.5 to 4 for 12 h of storage (with a step of 0.1). These ranges were selected in order to remain within realistic design configurations compared currently established

CSP plants. The parameters exhibit a perfect linear dependence ($R^2 > 0.99$), i.e. a et b are interpolated as linear functions of the solar multiple. The function for the evolution of the efficiency that we proposed in this study is therefore of the following form:

$$\eta(\text{DNI, SM}) = (a_1\ \text{SM} + a_2)\ \ln(\text{DNI}) + (b_1\ \text{SM} + b_2) \tag{7}$$

With the parameters a_1, a_2, b_1 and b_2 estimated for each technology with a large set of simulations (Table 6).

The efficiency is maximised for low values of the solar multiple such that the configurations allow to convert almost all incoming solar radiation into electricity. From an economic point a view they are not optimal as the power block and storage system are underused, yet from an energetic point of view, the optimal SM maximises the energy output.

2.6. Net energy and EROI values

A value for the global solar potential and EROI values in each geographical cell was calculated for the five technologies presented in Section 2.4. The net energy potential for each cell and for each country is evaluated as follows [22]:

$$\text{Net Energy Produced} = \text{Gross Energy Produced} - \sum \text{Energy Inputs} \tag{8}$$

With gross energy produced calculated based on Eq. (2) using the life time of the facility, and the energy inputs as evaluated in Section 2.2.

The EROI is calculated as the ratio of gross energy produced to energy inputs, i.e. in cell/country i:

$$\begin{aligned}\text{EROI} &= \frac{\text{Gross Energy Produced}}{\text{Energy Inputs}} \\ &= \frac{\text{Suitable Area}_i \cdot I_i \cdot \eta(I_i, \text{SM}_i) \cdot \text{GCR} \cdot \text{Life Time}}{\text{Energy Inputs}(\text{Rated Power, Aperture Area})}\end{aligned} \tag{9}$$

With the suitable area as a geographic constraint evaluated in Section 2.1, I_i the physical constraint of GHI/DNI of the location depending on the technology as evaluated in Section 2.2, η the solar-to-electric efficiency (depending on the irradiance and solar multiple for CSP applications), and GCR the ground cover ratio as technology constraints which were described in Section 2.3.

In case of CSP power plants the efficiency parametrisation from SAM simulations, as described in Section 2.5was combined with the detailed life cycle inputs data from Section 2.4 in a dynamic manner. The energy inputs were divided in a fixed part linked to the power block and thermal storage, and a variable part linked to the mirror field, so as to obtain cell specific energy inputs fitting with optimised solar multiples. The EROI of each CSP power technology was subsequently calculated for each DNI and solar multiple per cell by selecting the solar multiple that maximises the EROI. The optimal solar multiple as a function of the DNI is shown in Fig. 5 for the 3 CSP technologies, as well as the solar multiple that maximises the net energy produced per unit of
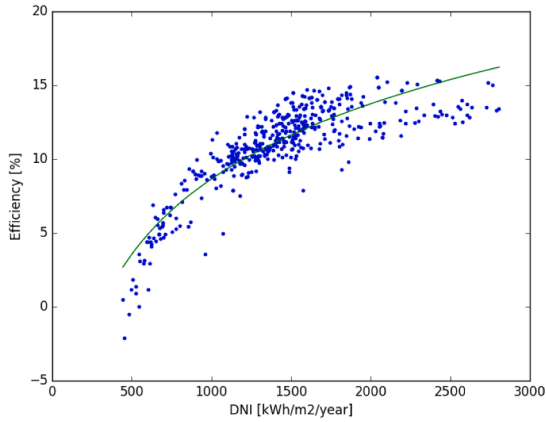
(a) PT-oil, solar mutliple = 1.3
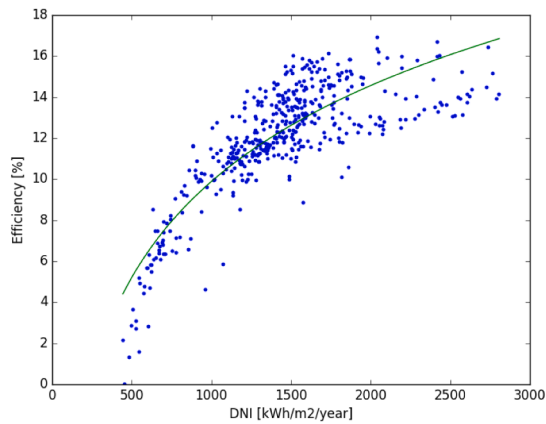
(b) PT-salt-TES, solar multiple = 2.7
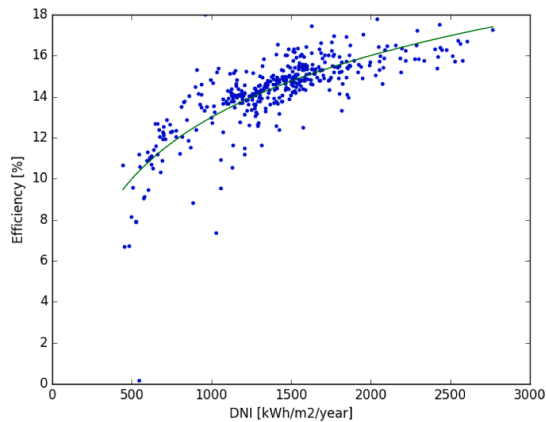
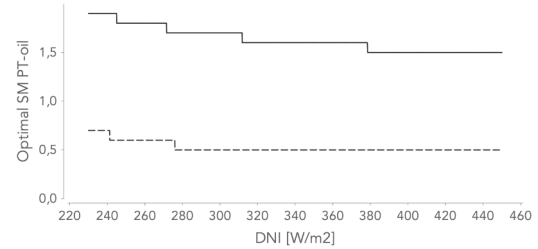

(c) ST-Salt-TES, solar multiple = 2.7

Fig. 4. Evolution of the efficiency with annual DNI, for PT-oil with a solar multiple of 1.3, and PT-Salt-TES and ST-Salt-TES with a solar multiple of 2.7, interpolated with the logarithmic function $\eta = 7.349\ln DNI - 42.12$, $\eta = 6.747\ln DNI - 36.72$, and $\eta = 4.339\ln DNI - 16.97$.

area. The solar multiple was set to a maximum for ST-Salt-TES in order to remain within realistic designs, such as due to growing atmospheric attenuation losses when allowing the distance between the heliostats and receiver to grow without bounds. The maximum was set to 4 for installations with 12 h storage corresponding to the change in slope in

Table 6
Parameters for Eq. (7) for each technology, with DNI expressed in kWh/m²/year.

	a_1	a_2	b_1	b_2
PT-oil	−3.38	11.55	23.85	−72.26
PT-Salt-TES	−1.578	11.17	10.65	−66.33
ST-Salt-TES	−1.62	8.742	11.01	−46.86

(a) PT-oil
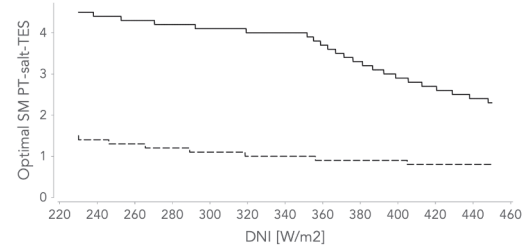
(b) PT-Salt-TES
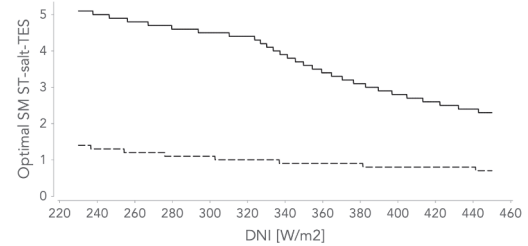
(c) ST-Salt-TES

Fig. 5. Solar multiple maximising the EROI or the net energy production of the installation as a function of the annual DNI.

Fig. 5. The slope change is observed because at higher solar multiple there is considerable curtailment where energy captured by the heliostat exceeds the power block and storage capacity.

2.7. Global EROI constraints

The resulting outputs from Eq. (8) for net energy potential and Eq. (9) for EROI were combined to establish a function depicting the evolution of the EROI with the net energy potential, similar to the methodology in [22]. The function classifies geographies or countries by decreasing EROI and then draws the evolution of EROI with the cumulative net energy potential. The total net energy production potential is plotted on the x-axis against the associated EROI on the y-axis. The shape of the curve provides insights in the repartition of the resources. If, for example, the initial decrease is steep it implies hat high EROI

resources for solar power limited on earth. On the opposite, if there is a large plateau at high EROI, it implicates that many geographies suitable for extracting energy from solar radiation at low energy input requirements compared to energy ouputs generated. In addition, the function allows for selecting a net energy constraint by allowing partitioning of the cumulative net energy resource at an EROI cut-off threshold for what energy resource is extracted. Cut-offs were selected based on the shape of the function at EROI values equal or greater than 5, 7.5 and 9, to establish the variation in net energy solar resource. The procedure was carried out for each of the individual technologies. In addition, to obtain a globally integrated picture based on a selection of solar technologies which are optimal for each location, one of the five technologies was selected based on which provided the highest EROI value in that cell.

3. Results

Before evaluating global grid cell multi-constrained results, a summary of results for each of the five solar technology systems at 1 GW scale is first presented. To create a fair comparison the results are presented when operating under the same irradiance conditions corresponding to Sevilla, Spain at a yearly averaged GHI of 207 W/m^2, and a yearly averaged DNI of 237 W/m^2. In Table 7 solar-PV and CSP technology system results can be found for area occupied, solar-to-electric efficiency, capacity factor, life time energy inputs and outputs, and EROI. Among PV technologies, mono-Si-PV based on the specifications has a higher EROI and energy production density due to its greater efficiency, despite higher energy inputs. In case of CSP technologies, the high energy cost of synthetic oil HTF negatively impacts the EROI of PT-oil compared to PT-Salt-TES [84]. ST-Salt-TES exhibits the best conversion efficiency at similar energy inputs needs PT-Salt-TES. The high capacity factor provided by CSP plants with storage gives these technologies additional benefits for electricity systems, despite their lower EROI. However, the capacity factor was not included as a driving variable in the multi-constraints optimisation model to select the best technology for each location.

3.1. Technology comparison at 1 GW scale

#### 3.1.1. Global large scale ground systems net energy potential

The result for the available energy that can be extracted from solar power is presented in this section, based on the mapping of EROI to cumulative net energy, as described in Section 2.7. The resulting function is shown for each individual technology in Fig. 6. The total global net potential for each individual technology was evaluated at 811, 1194, 234, 261, and 294 EJ/year for poly-Si-PV, mono-Si-PV, PT-oil, PT-Salt-TES, and ST-Salt-TES, respectively. In comparison, world final energy consumption in 2016 was estimated at 96 Mtoe (~400 EJ). The potential for CSP is significantly lower than for solar PV from an individual perspective because of slope restrictions and higher ground cover ratios. The curves show that the best geographic sites for these technologies have an EROI at 9, 10.4, 8.2, 8.5 and 9 for poly-Si-PV,
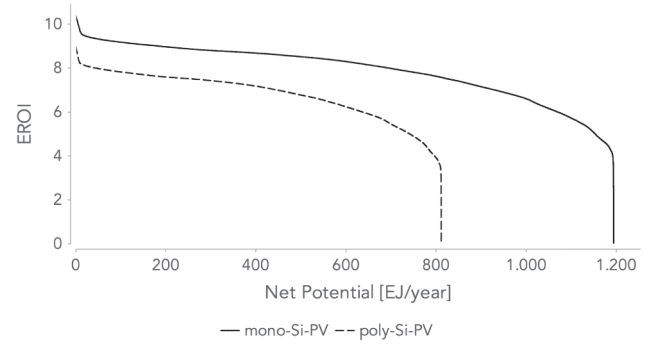
(a) Global potential for the different PV technologies
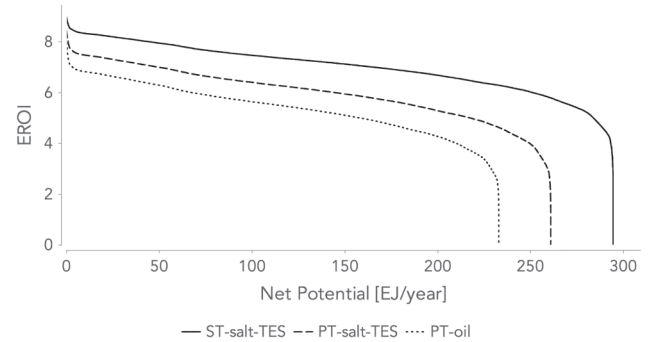
(b) Global potential for the different CSP technologies
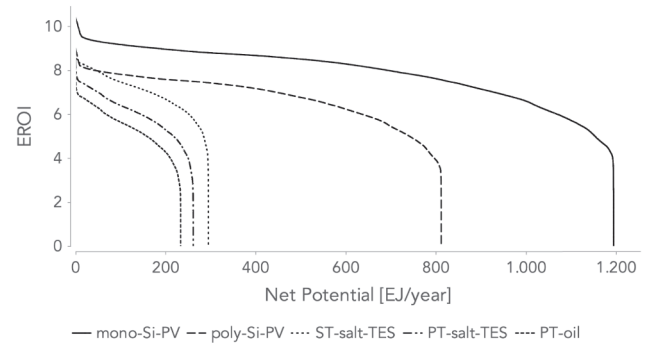
(c) Global potential for all solar technologies

Fig. 6. Global solar net energy potential for the different technologies considered in this study.

mono-Si-PV, PT-oil, PT-Salt-TES, and ST-Salt-TES, respectively.

The global net potential was also calculated by choosing, for each cell, the technology with the highest EROI, see Fig. 7. The total global net potential with the best technology in each cell was evaluated at

Table 7
Life cycle inputs, outputs and EROI of 1 GW installed for the 5 technologies, with irradiance conditions corresponding to Sevilla, Spain (a yearly averaged GHI of 207 W/m^2, and a yearly averaged DNI of 237 W/m^2).

|	poly-Si-PV	mono-Si-PV	PT-oil		PT-Salt-TES		ST-Salt-TES	
Solar multiple (usual/optimised)	–	–	1.3	1.9	2.7	4	2.7	4
Area occupied [km^2]	29	21	47	68	97	144	102	150
$\eta_{solar \to elec}$ [%]	13	18.6	13	11.9	14.8	13	15.8	14
Capacity Factor [%]	15.8	16.1	19	26	45	59	50	67
Lifetime outputs [PJ]	124.9	126.9	181	242	427	557	478	630
Lifetime fixed inputs [PJ]	18.73	16.2	21.6	27.7	43.5	51.6	36.9	42.6
EROI	7.1	8.2	5.2	5.3	5.7	6	6.7	7
Energy production density [W$_e$/m^2]	5.4	7.7	4.1	3.7	4.7	4.1	5	4.4
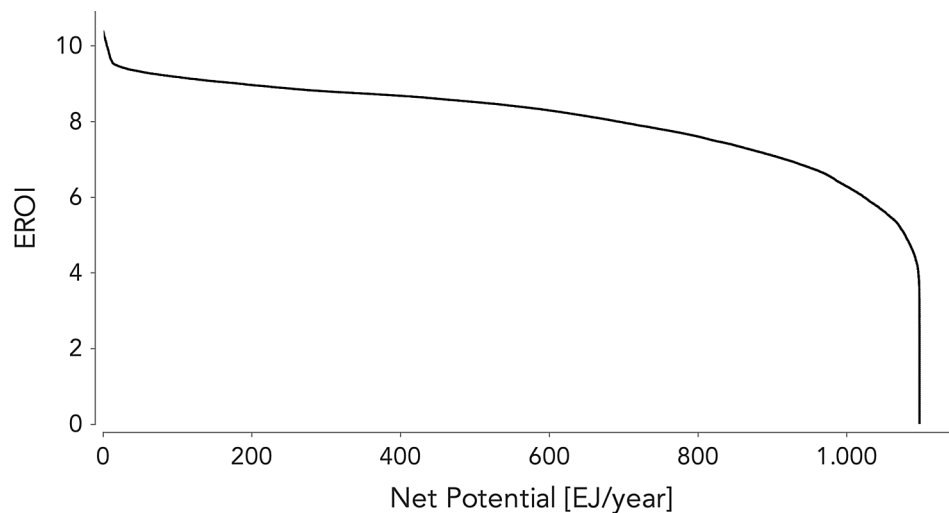
Fig. 7. Global solar potential as a decreasing function of the EROI, obtained by selecting the technology with the highest EROI in each cell.

1098 EJ/year and is dominated by the selection of mono-Si-PV technologies. It is lower than the global potential of mono-Si-PV if selected alone without other technologies, because CSP provides for a better EROI in cells with very high DNI levels, yet has a lower production per unit of area due to a larger ground cover ratio.

3.1.1.1. Impacts of EROI constraints on the net energy potential. The evaluation found that of the total net energy potential 98% or 1076 EJ/year can be obtained at EROI greater than 5, 75% or 823.5 EJ/year at an EROI greater than 7.5, and 15% or 164.7 EJ/year at an EROI greater than 9 Fig. 11. The results indicate that large areas of land are available with a good solar resource quality. In contrast, a similar grid cell method for the global net wind energy potential [31] resulted in a far steeper decline in EROI. A key difference is that there are large areas with the highest resource, such as high solar radiation areas like deserts, which are in general not suitable for human activities, i.e. thereby suitable for large solar power plants.

As discussed in the introduction Section 1, the threshold represents a minimum EROI that needs to be maintained for societies economic balance to continue, without requiring to shift capital from non-energy sectors to energy sector. The minimum EROI that a sustainable society must have is difficult to estimate and an on-going research effort [25]. Here EROI thresholds were chosen as outlined in Section 2.7 based on changes in the steepness of the curves, to explore points at which the net energy potential changes significantly when the minimum EROI requirement increases.

3.1.1.2. Impact of the CSP solar multiple design optimisation. In Fig. 8 the impact of the design optimisation is presented. For each type of CSP technology the global net energy potential as a function of EROI was drawn. Both with a standard solar multiple and an optimal SM value as described in Table 7. In case of CSP technologies without storage there is almost no difference as the model will select similar solar multiples in both the standard and optimal case. For model runs with 12 h of storage capacity the curve with the optimal solar multiples delivers marginally higher EROIs, yet at a cost of 30 EJ of lower global net energy potential due to the greater land occupation as a consequence of the higher solar multiple.

3.2. Global solar PV rooftop net energy potential

The results provide for a global net energy potential is split into residential and commercial rooftops, respectively. The values are 28.1 and 28.86 EJ/year for 24% efficient mono-Si-PV, and 19.06 and 19.54 EJ/year for 17% efficient poly-Si-PV. Results are presented as a

function of the decreasing EROI in Fig. 9. Despite high variations in usability factors, as defined in Section 2.1, the total suitable residential and commercial rooftop areas are similar. Compared to the ground mounted power plant potential, the rooftop solar potential is less than 5% of the global potential for both PV technologies (39 EJ/year compared to 811 EJ/year for poly-Si-PV, and 57 EJ/year compared to 1194 EJ/year for mono-Si-PV). Based on these results theoretically rooftop solar could provide for 7.5% of the current world's energy needs, indicating that both rooftop and ground mounted solar power systems are required in a renewable energy transition.

The combined value in this study for mono-Si-PV is 32% of the joint 102.5 EJ/year potential for residential buildings and 46.7 EJ/year for commercial buildings, as estimated by [5], despite using similar 24% efficiency solar modules. The results in this study are significantly lower due to more conservative usability factors (see Section 2.1) and conversion efficiencies.

3.3. Resulting spatial distribution of the solar resource

In order to analyse areas with the highest potential and the areas that would need to be covered with power plants, the simulation results are presented on a geographic map of the world in Figs. 11. The results are presented for three cases using the selected thresholds at an EROI of 5 (98% of the global potential), 7.5 (75% of the global potential) and 9 (15% of the global potential) as defined in Section 2.7. The technology selected by the model in each cell (i.e. the one maximising the EROI) is represented: areas in blue for PV and areas in orange for CSP. The comparison shows that a large part of the potential is realised at low EROIs. When the minimum EROI requirement is increased to 7.5 the net energy potential is reduced drastically in Europe, China, South-East Asia, Japan, North America, and Russia. At a minimum EROI requirement of 9 only Chile, countries in the eastern Sahel region, Namibia, Somalia, Saudi-Arabia, Oman and Yemen, and Western Australia still possess significant solar net energy potential.

Most of the time, mono-Si solar PV performs better than CSP, except in very high solar radiation regions including the USA, south of Chile and Argentina, Australia, western China, Kazakhstan and Mongolia Fig. 11. When the EROI threshold increases, the fraction of the potential viable with CSP significantly decreases, until eventually there is no CSP left at an EROI threshold of 9. In Fig. 12, the results were computed with poly-Si-PV as the unique PV technology. The results differ significantly, since for poly-Si-PV the EROIs of CSP and PV are similar. In contrast to the previous results, CSP is now preferred to solar-PV in Chile, the American Southwest, South Africa, and Australia. In the last map, showing the available solar potential at an EROI ⩾ 8 (15% of the
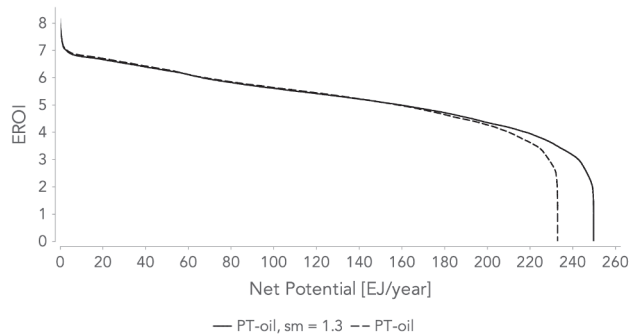
(a) PT-oil
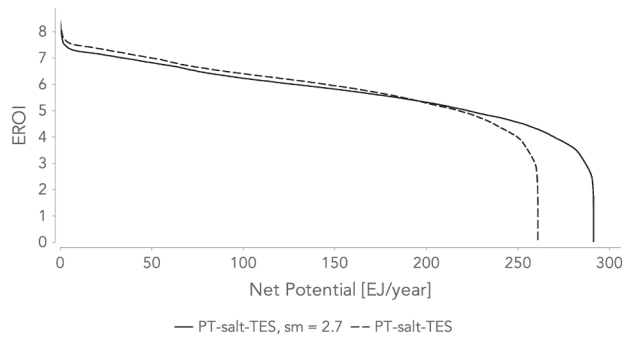
(b) PT-Salt-TES
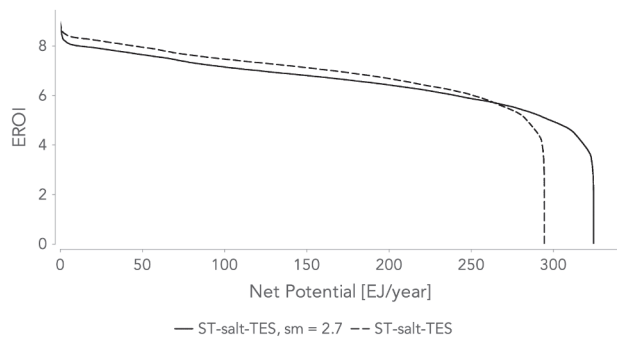
(c) ST-Salt-TES

Fig. 8. Global solar net energy potential for each CSP technology, with the usual solar multiple (1.3 without storage and 2.7 with a storage capacity of 12 h) and with the solar multiple optimised by the model.

global potential), almost no PV is viable.

3.4. Results split by regions

This global potential is further split by continent in Fig. 10 and Table 8. The potential of the African continent drives the global curve with 37% to 40% of the global solar net energy potential, followed by Asia at 25% to 30% of the potential solar net energy potential. A comparison of the EROI dependent net energy curves between continents shows an almost horizontal curve for the African continent and an almost vertical curve for the European continent, emphasising the uneven quality distribution of the solar power resources on earth.

In Table 9, it can be seen that when the EROI threshold is set to 9, the share of the potential of the African continent increases to 67% (mainly from the Sahara as per Fig. 11), followed by a share of 19% from the Asian continent.
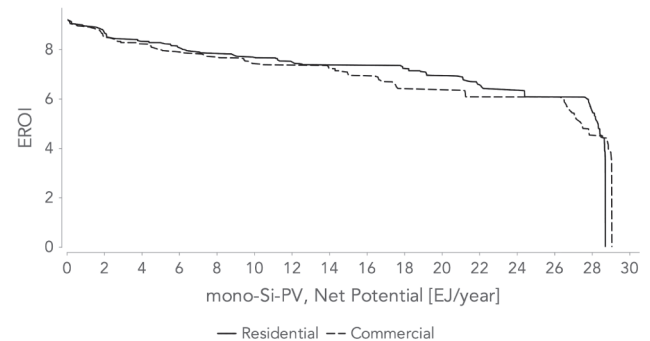
(a) mono-Si-PV
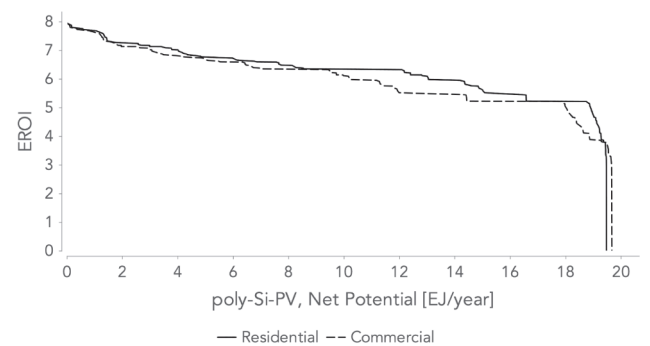
(b) poly-Si-PV

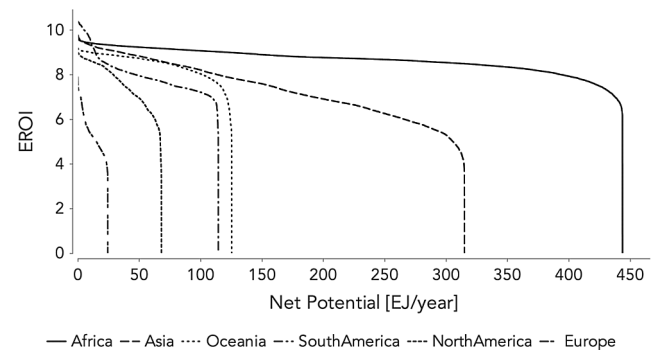**Fig. 9.** Residential and commercial rooftop solar PV net energy potentials.

Fig. 10. Global solar net energy potential split by continent.

3.4.1. EU-28 countries

Individual results for the EU-28 countries are shown in Fig. 13. The net potentials for each individual technology evaluated in isolation as if solely deployed was established at 13, 19, 2, 2, and 3 EJ/year for poly-Si-PV, mono-Si-PV, PT-oil, PT-Salt-TES, and ST-Salt-TES, respectively. As presented in Table 8, the potential of the European continent represents only 2% of the global potential. In addition, the EROI of the resource are lower and decreasing faster, indicating substantial limitations to the expansion of solar power to provide a significant part of European energy needs.

3.5. Discussion

3.5.1. Limitations of the study design

The study provides estimates for different geographies and countries, yet in certain cases it is potentially biased due to the use of average non-country specific factors. This is especially the case for rooftop solar-PV estimations, where average values were used to estimate the proportion of rooftop area that is applicable to solar-PV
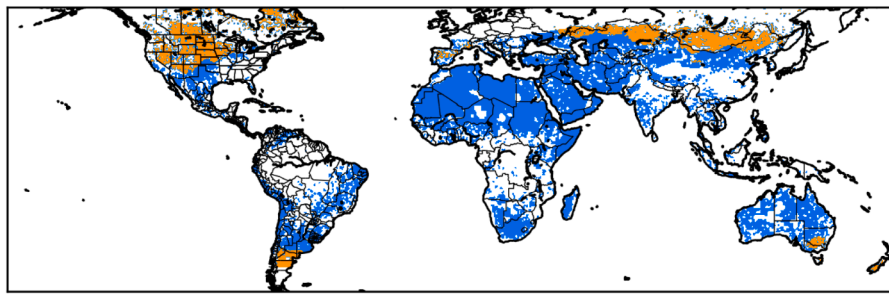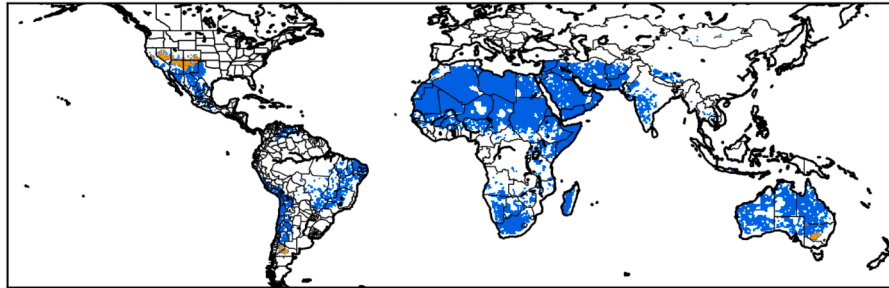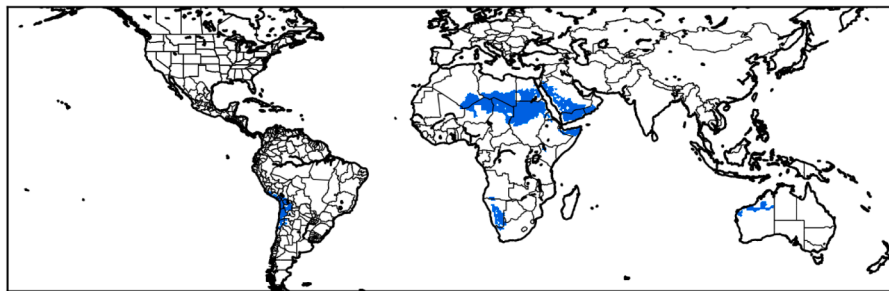
(a) EROI $\geq$ 5, 98% of the global potential

(b) EROI $\geq$ 7.5, 75% of the potential

(c) EROI $\geq$ 9, 15% of the potential

Fig. 11. Spatial distribution of the potential, with mono-Si-PV as PV technology. The areas in blue are the areas where mono-Si-PV performs better than CSP, and orange the opposite. The areas with a solar potential are presented for increasing values of the minimum EROI required, from top to bottom.

systems, as derived from the literature. Further studies that provide better granularity for such averages, like country by country studies of typical building typologies to derive suitability of solar-PV systems would be helpful to reduce the uncertainty of this assumption.

Working with EROI as the only decision variable for the choice of a type of technology (i.e. PV or CSP) and the optimal design of a power plant (i.e. the selection of the solar multiple for CSP power plants) has shown some limitations. Regarding the type of technology, the model is currently not able to take into account the capacity factor in its selection. While the need for storage remains small under the current global share of renewable energy, it will increase significantly as renewable energies grow in the mix, negatively impacting the EROI [85]. As such, comparing solar-PV power plants with CSP power plants with 12 h of thermal energy storage can result in an apples with pears comparison.

In theory, CSP technologies with storage could allow for reaching capacity factors close to 100%, yet only one system in practice has attained a 75% capacity factor and more typical storage coupled systems have a capacity factor below 50% at present [86]. CSP technologies are potentially more suitable for baseload generation than solar-PV power plants without storage, whose capacity factors do not exceed

24%. Further analysis is needed to understand the effect of introducing significant battery storage for solar-PV on the global energy potential with EROI constraints, such as the effect of batteries on the EROI value of solar-PV power plants. To implement this a temporally solved simulation is required that takes into account hourly dynamics.

The research is also limited in its application to existing commercial solar technologies, whilst new cell types could provide promising low energy costing high efficiency routes to extract more of the global solar resource. In particular perovskite cells and dye-sensitized solar cells would have been interesting technologies to assess in how they would in theory change the global net solar energy potential. Available data to adequately assess these technologies is still limited however, with no manufacturing scale energy input data being available for adequate assessment.

Regarding the design of CSP power plants, the EROI maximisation will always select larger aperture areas than current systems until the marginal cost of an additional mirror is higher than surplus production generated. The reason is the absence of costs associated to land use in the model. An additional constraint that specifies the area occupied by power plants within the model as a dynamic factor instead of a static
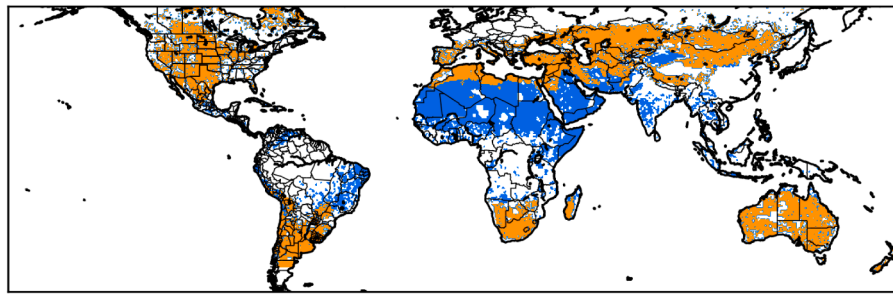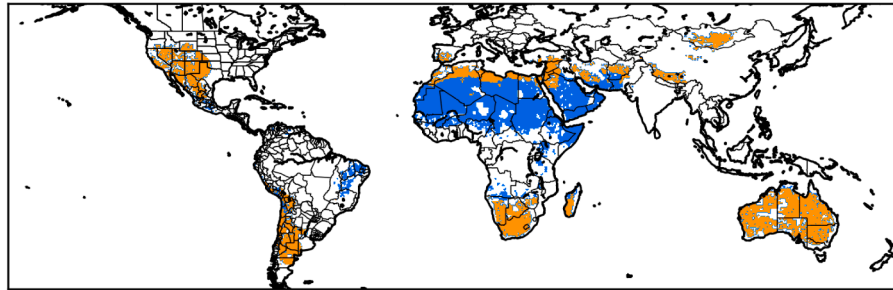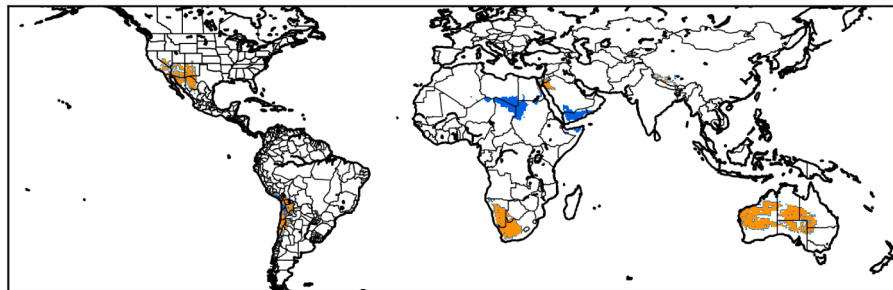
(a) EROI $\geq$ 5, 97% of the global potential

(b) EROI $\geq$ 7, 70% of the global potential

(c) EROI $\geq$ 8, 15% of the global potential

Fig. 12. Spatial distribution of the potential, with poly-Si-PV as unique PV technology. The areas in blue are the areas where poly-Si-PV performs better than CSP, and orange the opposite. The areas with a solar potential are presented for increasing values of the minimum EROI required.

Table 8
Global potential split by continent without an EROI threshold, all values in EJ/year.

Continent/EJ/year	Total	% of Total	PV	% of PV	CSP	% of CSP
Africa	444	40	444	37	112	38
Asia	315	29	361	30	72	25
Oceania	125	11	129	11	55	19
South America	114	10	120	10	23	8
North America	68	6	106	9	25	8
Europe	24	2	27	2	4	1
Total	**1099**	–	**1194**	–	**294**	–

Table 9
Global potential at EROI $\geqslant$9, split by continent, all values in EJ/year. The table contains solar-PV values only since the CSP resource potentials viable at this EROI threshold are negligible.

Continent	Total (PV only)	% of Total
Africa	124	67
Asia	35	19
Oceania	11	6
SouthAmerica	14	8
NorthAmerica	0	0
Europe	0	0
Total	**184**	**100**

one should be developed to overcome this limitation.

In terms of the overall study methodology, the use of a static approach can be questioned as it does not take into account the annual evolution of the energy system within an energy transition context. Follow-up research would be needed to integrate a dynamic approach to take into account the evolution in primary and final energy needs, taking into account factors such as the decrease of primary energy inputs due to the electrification of the energy system.

3.5.2. Comparison of results

The results obtained here can be compared with results from previous studies (Table 1). The global potential obtained is similar to the results from [15] of 1300 EJ/year, when no restriction is applied on the minimum EROI required, and significantly lower than all the other estimates, except the results for the top-down approach by [18]. The results demonstrate that it is important to take into account energy
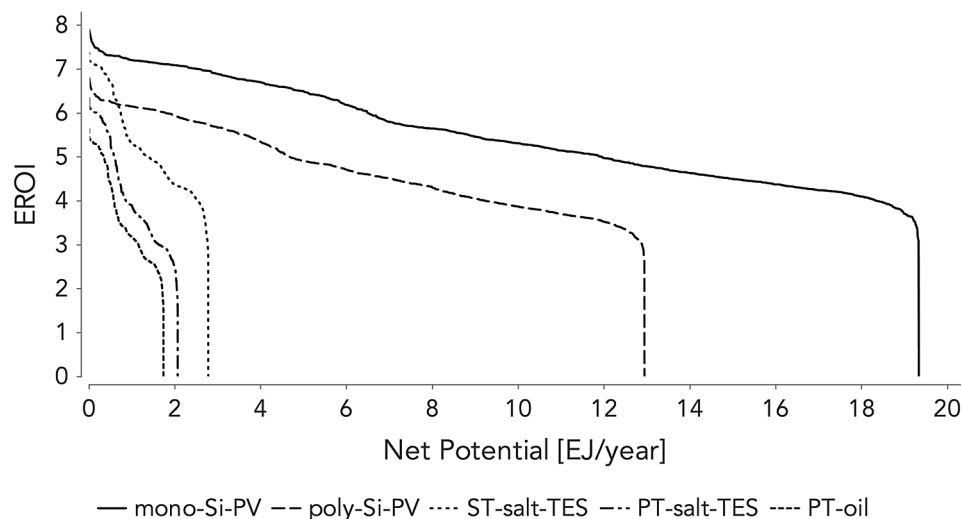
Fig. 13. EU-28 countries solar net energy potential evaluated with the studies multi-constraints model.

input requirements when assessing the available potential of a renewable resource.

4. Conclusions

The study provides a novel methodology to integrate land, physical solar resource, solar technology constraints, and net energy constraints, so as to estimate the global solar energy potential. It is also the first to provide an integrated estimate for both solar photovoltaic and concentrated solar power in the analysis, including currently commercialised and state of the art technologies. And a new parametrisation has been outlined for concentrated solar power power plants. The final results are a series of solar net energy potential curves, with the cumulative global available solar potential on the x-axis and the corresponding energy return on energy investment level plotted on the y-axis.

The global net energy potential, as the amount of energy available after substracting the energy invested for the infrastructure and operation, was established as follows:

- Solar-PV:
  - Monocrystalline silicon photovoltaic power plant with 24% efficiency: 1194, 1153, 828, and 184 exajoules per year, at energy return on energy investment thresholds of 1, 5, 7.5, and 9, respectively.
  - Polycrystalline silicon photovoltaic power plant with 17% efficiency: 811, 741, 263, and 0 exajoules per year, at energy return on energy investment thresholds of 1, 5, 7.5 and 9, respectively.
- Concentrated Solar Power:
  - Parabolic trough power plant with oil heat transfer fluid: 234, 159 and 1 exajouler per year, at energy return on energy investment thresholds of 1, 5, and 7.5, respectively.
  - Parabolic trough power plant with molten salt and 12 h of thermal energy storage capacity: 161, 218, and 8 exajouler per year, at energy return on energy investment thresholds of 1, 5, and 7.5, respectively.
  - Solar tower power plant with molten salt and 12 h of thermal energy storage capacity: 294, 284, and 96 exajouler per year, at energy return on energy investment thresholds of 1, 5, and 7.5, respectively.
- Integrated solar technologies based on selecting the highest energy return on energy investment providing cells:
  - Primarily dominated by Monocrystalline silicon photovoltaic plants combined with Solar tower power plant with molten salt

heat transfer fluid: 1098 exajoules per year

Although many studies conclude that the available solar potential will not be a limiting factor for renewable energy development, this study shows that the energy inputs, i.e. the capital stock and operational requirements of the energy sector that would have to be mobilised, could require a significant shift of efforts from non-energy sectors to the energy sector, which plausibly would have significant economic impacts, especially for low quality solar resource regions such as the European countries.

Further work can explore three different aspects. A combination of the results for wind and solar power potential would be worthwhile, also including additional storage technologies, so as to better evaluate the extent to which they would be complementary from an geographic and energy return on energy investment perspective. As these two sources of energy are seen as the most promising in order to build a sustainable energy system, this kind of work is essential to build forward looking energy scenarios based on realistic available resource potentials per country and geography. Especially with the perspective of the journal Applied Energy to assess the application potential of different energies, which can feed into the setting of renewable energy targets in the policy agenda.

A second route for further research is needed to reduce the ambiguity on what energy return on energy investment cut-off level would be desirable from a societal perspective, to prevent significant implications of the energy system performance falling below the required energy return on energy investment cut-off. Having an understanding of such thresholds would greatly increase the usefulness of the research for sustainable energy systems design. Finally, the research can be expanded by including novel solar technologies once sufficient energy input and technology data is available, such as perovskite cells and dye-sensitized solar cells.

References

[1] Hall Charles AS, Day John W. Revisiting the limits to growth after peak oil. Am Sci 2009.
[2] OECD/IEA and IRENA. Perspectives for the Energy Transition: Investment Needs for a Low-Carbon Energy System. Technical report, International Energy Agency and International Renewable Energy Agency, Paris; 2017.
[3] Geels Frank W. Disruption and low-carbon system transformation: progress and new challenges in socio-technical transitions research and the Multi-Level Perspective. Energy Res Soc Sci 2018;37(September 2017):224–31.
[4] IEA. World Energy Outlook 2017. Technical report, International Energy Agency; 2017.
[5] Jacobson Mark Z, Delucchi Mark A, Bauer Zack AF, Goodman Savannah C, Chapman William E, Cameron Mary A, et al. 100% Clean and renewable wind,

water, and sunlight all-sector energy roadmaps for 139 countries of the world. Joule 2017;1(1):108–21.

[6] Ram M, Bogdanov D, Aghahosseini A, Gulagi A, Oyewo SA, Child M, et al. Global Energy System based on 100% renewable energy: Power, Heat, Transport and Desalination Sectors. Technical Report April, Lappeenranta, Berlin; 2019.

[7] Brown TW, Bischof-Niemz T, Blok K, Breyer C, Lund H, Mathiesen BV. Response to 'Burden of proof: a comprehensive review of the feasibility of 100% renewable-electricity systems. Renew Sustain Energy Rev 2018;92(September 2016):834–47.

[8] Clack Christopher TM, Qvist Staffan A, Apt Jay, Bazilian Morgan, Brandt Adam R, Caldeira Ken, et al. Evaluation of a proposal for reliable low-cost grid power with 100% wind, water, and solar. Proc Natl Acad Sci 2017;114(26):6722–7.

[9] Heuberger Clara Franziska, Dowell Niall Mac. Real-World Challenges with a Rapid Transition to 100% Renewable Power Systems. Joule 2018;2(3):367–70.

[10] Rogner Hans-Holger, Aguilera Roberto, Archer Cristina L, Bertani Ruggero, Bhattacharya SC, Dusseault Maurice B, et al. energy resources and potentials convening lead author (CLA). In: Global energy assessment: towards a sustainable future. Austria, 1st ed.; 2012. p. 425–512 [chapter 7].

[11] Capellán-Pérez Iñigo, de Castro Carlos, Arto Iñaki. Assessing vulnerabilities and limits in the transition to renewable energies: land requirements under 100% solar energy scenarios. Renew Sustain Energy Rev 2017;77(December 2016):760–82.

[12] Dugaria Simone, Padovan Andrea, Sabatelli Vincenzo, Del Col Davide. Assessment of estimation methods of DNI resource in solar concentrating systems. Sol Energy 2015;121:103–15.

[13] Kabir Ehsanul, Kumar Pawan, Kumar Sandeep, Adelodun Adedeji A, Kim Ki Hyun. Solar energy: potential and future prospects. Renew Sustain Energy Rev 2018;82(September):894–900.

[14] Moriarty Patrick, Honnery Damon. Can renewable energy power the future? Energy Policy 2016;93:3–7.

[15] Hoogwijk Monique Maria. On the global and regional potential of renewable energy sources [PhD thesis]. Utrecht: Universiteit; 2004.

[16] Trieb Franz, Schillings Christoph, Sullivan Marlene O, Pregger Thomas, Hoyer-klick Carsten. Global potential of concentrating solar power. In: SolarPaces Conference Berlin, September 2009 Global, number September, Berlin; 2009. p. 1–11.

[17] GEA. Global Energy Assessment - Toward a Sustainable Future. Cambridge University Press, Cambridge, UK and New York, NY, USA and the International Institute for Applied Systems Analysis, Laxenburg, Austria; 2012.

[18] De Castro Carlos, Mediavilla Margarita, Miguel Luis Javier, Frechoso Fernando. Global solar electric potential: a review of their technical and sustainable limits. Renew Sustain Energy Rev 2013;28:824–35.

[19] Deng Yvonne Y, Haigh Martin, Pouwels Willemijn, Ramaekers Lou, Brandsma Ruut, Schimschar Sven, et al. Quantifying a realistic, worldwide wind and solar electricity supply. Glob Environ Change 2015;31:239–52.

[20] Hall Charles AS, Cleveland Cutler J. Petroleum drilling and production in the United States: yield per effort and net energy analysis. Science 1981;211(4482):576–9.

[21] Brandt Adam R, Dale Michael. A general mathematical framework for calculating systems-scale efficiency of energy extraction and conversion: energy return on investment (EROI) and other energy return ratios. Energies 2011;4(8):1211–45.

[22] Dale Michael, Krumdieck Susan, Bodger Pat. A dynamic function for energy return on investment. Sustainability 2011.

[23] Hall Charles A S. Will EROI be the primary determinant of our economic future? The view of the natural scientist versus the economist. Joule 2017;1(4):635–8.

[24] King Lewis C, Van Den Bergh Jeroen CJM. Implications of net energy-return-on-investment for a low-carbon energy transition. Nat Energy 2018;3(4):334–40.

[25] Hall Charles AS, Balogh Stephen, Murphy David JR. What is the minimum EROI that a sustainable society must have? Energies 2009.

[26] Lambert Jessica G, Hall Charles AS, Balogh Stephen, Gupta Ajay, Arnold Michelle. Energy, EROI and quality of life. Energy Policy 2014;64:153–67.

[27] Kis Zoltán, Pandya Nikul, Koppelaar Rembrandt HEM. Electricity generation technologies: comparison of materials use, energy return on investment, jobs creation and CO2emissions reduction. Energy Policy 2018;120(May):144–57.

[28] Kunz Hannes, Hagens Nathan John, Balogh Stephen B. The influence of output variability from renewable electricity generation on net energy calculations. Energies 2014;7(1):150–72.

[29] Brandt Adam R, Englander Jacob, Bharadwaj Sharad. The energy efficiency of oil sands extraction: energy return ratios from 1970 to 2010. Energy 2013;55:693–702.

[30] Kumar Manish, Kumar Arun. Performance assessment and degradation analysis of solar photovoltaic technologies: a review. Renew Sustain Energy Rev 2017;78(April):554–87.

[31] Dupont E, Koppelaar R, Jeanmart H. Global available wind energy with physical and energy return on investment constraints. Appl Energy 2018;209.

[32] ESA and UCL. GlobCover 2009 (Global Land Cover Map); 2009. http://due.esrin.esa.int/page_globcover.php.

[33] IUCN and UNEP-WCMC. The World Database on Protected Areas (WDPA); 2016. www.protectedplanet.net/.

[34] VLIZ. Union of the ESRI Country shapefile and the Exclusive Economic Zones (version 2); 2014. http://www.marineregions.org/.

[35] Guerin Turlough F. Impacts and opportunities from large-scale solar photovoltaic (PV) electricity generation on agricultural production. Environ Qual Manage 2019;28(4):7–14.

[36] Brewer Justin, Ames Daniel P, Solan David, Lee Randy, Carlisle Juliet. Using GIS analytics and social preference data to evaluate utility-scale solar power site suitability. Renew Energy 2015;81:825–36.

[37] Fischer G, Nachtergaele F, Prieler S, van Velthuizen HT, Verelst L, Wiberg D. Global Agro-ecological Zones Assessment for Agriculture. Technical report, IIASA, Laxenburg, Austria and FAO, Rome, Italy; 2007.

[38] Enerdata. Entranze Building floor area per capita; 2019.

[39] Melius J, Margolis R, Ong S. Estimating rooftop suitability for PV: a review of methods, patents, and validation techniques. Natl Renew Energy Lab 2013;(December)35.

[40] World Bank Group ESMAP. Global Solar Atlas; 2019.

[41] Oliver Knight. Assessing and Mapping Renewable Energy Resources. Technical report, World Bank Group, Washington DC; 2016.

[42] Skoplaki E, Palyvos JA. On the temperature dependence of photovoltaic module electrical performance: a review of efficiency/power correlations. Sol Energy 2009;83(5):614–24.

[43] Wang Xiaoting, Barnett Allen. The evolving value of photovoltaic module efficiency. Appl Sci 2019;9(6):1227.

[44] J. Trube, ITRPV, and VDMA. International Technology Roadmap for Photovoltaic (ITRPV): 2018 Results. Technical report, VDMA; 2016.

[45] Cao Yu, Shengzhi Xu, Yao Jianxi, Han Shuwei. Recent advances in and new perspectives on crystalline silicon solar cells with carrier-selective passivation contacts. Crystals 2018;8(11):430.

[46] Fthenakis VM, Frischknecht R, Raugei M, Kim HC, Alsema E, Held M, et al. Methodology guidelines on life cycle assessment of photovoltaic electricity. Methodology guidelines on life cycle assessment of photovoltaic electricity. IEA PVPS T(5454): International Energy Agency Photovoltaic Power Sys; 2011.

[47] Leloux Jonathan, Taylor Jamie, Moretón Rodrigo, Narvarte Luis, Trebosc David, Desportes Adrien, et al. Monitoring 30,000 PV systems in Europe: performance, faults, and state of the art. In: 31st European photovoltaic solar energy conference and exhibition, (September); 2015. p. 1574–82.

[48] Taylor Jamie, Leloux J, Hall LMH, Everard AM, Briggs J, Buckley A. Performance of distributed PV in the UK: a statistical analysis of over 7000 systems. In: 31st European photovoltaic solar energy conference and exhibition, number September; 2015. p. 2263–8.

[49] Reich Nils H, Mueller Bjoern, Armbruster Alfons, Van Wilfried GJHM, Sark Klaus Kiefer, Reise Christian. Performance ratio revisited: is PR > 90% realistic? Prog Photovolt Res Appl 2012;20(6):717–26.

[50] Sakarapunthip Nattakarn, Chenvidhya Dhirayut, Chuangchote Surawut, Kirtikara Krissanapong, Chenvidhya Tanokkorn, Onreabroy Wandee. Effects of dust accumulation and module cleaning on performance ratio of solar rooftop system and solar power plants. Jpn J Appl Phys 2017;56(8).

[51] Romero-Fiances Irene, Muñoz-Cerón Emilio, Espinoza-Paredes Rafael, Nofuentes Gustavo, De La Casa Juan. Analysis of the performance of various pv module technologies in Peru. Energies 2019;12(1).

[52] Edalati Saeed, Ameri Mehran, Iranmanesh Masoud. Comparative performance investigation of mono- and poly-crystalline silicon photovoltaic modules for use in grid-connected photovoltaic systems in dry climates. Appl Energy 2015;160:255–65.

[53] Li Chong. Comparative performance analysis of grid-connected PV power systems with different PV technologies in the hot summer and cold winter zone. Int J Photoenergy 2018;2018.

[54] Hemanthbabu N, Shivashimpiger Sujata, Samanvita N, Parthasarathy VM. Performance ratio and loss analysis for 20MW grid connected solar PV system - case study. Int J Eng Adv Technol 2019;8(2):20–5.

[55] Sharma Vikrant, Chandel SS. Performance analysis of a 190kWp grid interactive solar photovoltaic power plant in India. Energy 2013;55:476–85.

[56] Arora Rajesh, Arora Ranjana, Sridhara SN. Performance assessment of 186 kWp grid interactive solar photovoltaic plant in Northern India. Int J Ambient Energy 2019;40:1–14.

[57] Yadav Satish Kumar, Bajpai Usha. Performance evaluation of a rooftop solar photovoltaic power plant in Northern India. Energy Sustain Develop 2018;43(February):130–8.

[58] Bhullar Sandeep Singh, Lalwani Mahendra. Performance analysis of 25 MW grid connected solar photovoltaic plant in Gujarat, India. 3rd International conference on innovative applications of computational intelligence on power, energy and controls with their impact on humanity, CIPECH 2018. IEEE; 2018. p. 20–5.

[59] Okello D, Van Dyk EE, Vorster FJ. Analysis of measured and simulated performance data of a 3.2 kWp grid-connected PV system in Port Elizabeth, South Africa. Energy Convers Manage 2015;100:10–5.

[60] Quansah David A, Adaramola Muyiwa S, Appiah George K, Edwin Isaac A. Performance analysis of different grid-connected solar photovoltaic (PV) system technologies with combined capacity of 20 kW located in humid tropical climate. Int J Hydrogen Energy 2017;42(7):4626–35.

[61] Halwachs M, Neumaier L, Vollert N, Maul L, Dimitriadis S, Voronko Y, et al. Statistical evaluation of PV system performance and failure data among different climate zones. Renew Energy 2019;139(March):1040–60.

[62] Jordan DC, Kurtz SR. Photovoltaic degradation rates – an analytical review. Prog Photovoltaics Res Appl 2013;21(1):12–29.

[63] CSP Bankability. Draft for an Appendix C - Solar Field Modeling to the SolarPACES Guideline for Bankable STE Yield Assessment. Technical Report 0325293; 2017.

[64] Islam Md Tasbirul, Huda Nazmul, Abdullah AB, Saidur R. A comprehensive review of state-of-the-art concentrating solar power (CSP) technologies: current status and research trends. Renew Sustain Energy Rev 2018;91(November 2017):987–1018.

[65] IRENA. Estimating the Renewable Energy Potential in Africa A GIS-based approach. Technical report, International Renewable Energy Agency; 2014.

[66] David Kearney. Utility-Scale Parabolic Trough Solar Systems: Performance Acceptance Test Guidelines: April 2009 - December 2010. Technical Report May, NREL, Oak Ridge; 2011.

[67] Blair Nate, Diorio Nicholas, Freeman Janine, Gilman Paul, Janzou Steven, Neises Ty, et al. System Advisor Model (SAM) General Description System Advisor Model (SAM) General Description (Version 2017.9.5). Technical Report May; 2018.

[68] Ong S, Campbell C, Denholm P, Margolis R, Heath G. Land-use requirements for solar power plants in the United States. Technical Report June; 2013.

[69] Koppelaar RHEM. Solar-PV energy payback and net energy: Meta-assessment of study quality, reproducibility, and results harmonization; 2017.

[70] Burkhardt John J, Heath Garvin, Cohen Elliot. Life cycle greenhouse gas emissions of trough and tower concentrating solar power electricity generation: systematic review and harmonization. J Ind Ecol 2012;16(SUPPL.1).

[71] Raugei Marco. Net energy analysis must not compare apples and oranges. Nat Energy 2019;4:86–8.

[72] BP. BP Energy Outlootk 2018 Edition. Technical report; 2018.

[73] Ohshita Y, Kamioka T, Nakamura K. Technology Trends of High Efficiency Crystalline Silicon Solar Cells. AAPPS Bulletin; 2017. p. 7.

[74] Hou Guofu, Sun Honghang, Jiang Ziying, Pan Ziqiang, Wang Yibo, Zhang Xiaodan, et al. Life cycle assessment of grid-connected photovoltaic power generation from crystalline silicon solar modules in China. Appl Energy 2016;164:882–90.

[75] Yu Zhiqiang, Ma Wenhui, Xie Keqiang, Lv Guoqiang, Chen Zhengjie, Wu Jijun, et al. Life cycle assessment of grid-connected power generation from metallurgical route multi-crystalline silicon photovoltaic system in China. Appl Energy 2017;185:68–81.

[76] Louwen A, Sark WGJHM, Schropp REI, Turkenburg WC, Faaij APC. Life-cycle greenhouse gas emissions and energy payback time of current and prospective silicon heterojunction solar cell designs. Prog Photovoltaics 2015;23:1406–28.

[77] Louwen A. Assessment of the energy performance, economics and environmental footprint of silicon heterojunction photovoltaic technology [PhD thesis]. University of Utrecht; 2016.

[78] Turchi Craig, Kurup Parthiv, Akar Sertac, Flores Francisco, Turchi Craig, Kurup Parthiv, et al. Domestic Material Content in Molten-Salt Concentrating Solar Power Plants Domestic Material Content in Molten-Salt Concentrating Solar Power Plants. Nrel/Tp-5500-64429, (August); 2015.

[79] Jorgenson Jennie, Denholm Paul, Mehos Mark, Turchi Craig. Estimating the Performance and Economic Value of Multiple Concentrating Solar Power Technologies in a Production Cost Model. (December); 2013.

[80] Raade Justin, Starns Travis, Martin Cam, Hanson Ron, Lagarenne Jon. Utilizing Molten Salt Energy Storage at Thermal Power Plants Halotechnics, Inc. – Corporate Profile; 2015. p. 1–19.

[81] Schuknecht Nathan, Mcdaniel Jennifer, Filas Harrison. Achievement of the $100/m 2 Parabolic Trough. In SolarPaces 2017, 26–29 September, Santiago, Chile; 2017. p. 8.

[82] Mathur A, Kasetty R, Oxley J, Mendez J, Nithyanandam K. Using encapsulated phase change salts for concentrated solar power plant. Energy Procedia 2013;49:908–15.

[83] Jacob Rhys, Martin Belusko A, Fernández Inés, Cabeza Luisa F, Saman Wasim, Bruno Frank. Embodied energy and cost of high temperature thermal energy storage systems for use with concentrated solar power plants. Appl Energy 2016;180:586–97.

[84] Batuecas E, Mayo C, Díaz R, Pérez FJ. Life Cycle Assessment of heat transfer fluids in parabolic trough concentrating solar power technology. Sol Energy Mater Sol Cells 2017;171(June):91–7.

[85] Limpens Gauthier, Jeanmart Hervé. Electricity storage needs for the energy transition: an EROI based analysis illustrated by the case of Belgium. Energy 2018;152:960–73.

[86] Boretti Albert, Castelletto Stefania, Al-Zubaidy Sarim. Concentrating solar power tower technology: present status and outlook. Nonlinear Eng 2019;8(10):10–31.